

The Occurrence and Properties of Long-Lived Liquid-Bearing Clouds over the Greenland Ice Sheet and Their Relationship to the North Atlantic Oscillation

JONATHAN EDWARDS-OPPERMAN

Cooperative Institute for Mesoscale Meteorological Studies, University of Oklahoma, Norman, Oklahoma

STEVEN CAVALLO

University of Oklahoma, Norman, Oklahoma

DAVID TURNER

NOAA/Earth Systems Research Laboratory/Global Systems Division, Boulder, Colorado

(Manuscript received 9 August 2017, in final form 22 January 2018)

ABSTRACT

Stratiform liquid-bearing clouds (LBCs), defined herein as either pure liquid or mixed-phase clouds, have a large impact on the surface radiation budget across the Arctic. LBCs lasting at least 6 h are observed at Summit, Greenland, year-round with a maximum in occurrence during summer. Mean cloud-base height is below 1 km for 85% of LBC cases identified, 59% have mean liquid water path (LWP) values between 10 and 40 g m⁻², and most produce sporadic light ice-phase precipitation. During their occurrence, the atmosphere above the ice sheet is anomalously warm and moist, with southerly winds observed over much of the ice sheet, including at Summit. LBCs that occur when the North Atlantic Oscillation (NAO) is in the negative phase correspond to strong ridging centered over the Greenland Ice Sheet (GIS), allowing for southwesterly flow over the GIS toward Summit. During the positive phase of the NAO, the occurrence of LBCs corresponds to a cyclone located off the southeastern coast of the ice sheet, which leads to easterly-to-southeasterly flow toward Summit. Furthermore, air parcels at Summit frequently originate from below the elevation of Summit, indicating that orographic lift along the ice sheet is a factor in the occurrence of LBCs at Summit. LBCs are more frequently observed during the negative NAO, and both the LWP and precipitation rate are larger in LBCs occurring during this phase. Mean LWP in LBCs occurring during the negative NAO is 15 g m⁻² larger than in LBCs occurring during the positive phase.

1. Introduction

The Arctic is warming at an accelerating rate relative to the rest of the globe (Serreze and Barry 2011). Understanding the various components of the Arctic climate system, and how they interact, is necessary in order to achieve a greater understanding of the observed changes in the region. The Greenland Ice Sheet (GIS) is a particularly important portion of the Arctic climate system because of its potential for further contributions to sea level rise (Shepherd et al. 2012) and its potential impact on the Atlantic meridional

overturning circulation (AMOC; Rahmstorf et al. 2015). As the Arctic continues to warm, it is imperative that a better understanding of Greenland's climate and the meteorological factors relating to the melt of the GIS is achieved.

Previous research concerning atmospheric influences on the GIS has noted the importance of the North Atlantic Oscillation (NAO). The negative phase of the NAO (−NAO) has been linked with the advection of warm, moist air masses over the ice sheet (Mosley-Thompson et al. 2005; Bromwich et al. 1999; Van Loon and Rogers 1978). During the −NAO, high pressure anomalies are present over the GIS with ridging and southwesterly flow dominant over much of the ice sheet. Research concerning low pressure anomalies in the region has largely focused on

Corresponding author: Jonathan Edwards-Opperman, jeo6@ou.edu

the relationship with precipitation over the GIS, especially that which falls on the periphery of the ice sheet since most of Greenland's precipitation falls along the southern and southeastern coasts (Schuenemann et al. 2009; Schuenemann and Cassano 2009). These precipitation maxima are related to the interaction between wind patterns induced by cyclones passing near the coast of Greenland and the steep slope of the terrain along the edge of the GIS (Schuenemann et al. 2009). Correspondence between the interaction of wind patterns with the terrain of the ice sheet and the occurrence of precipitation has been noted for some time (Ohmura and Reeh 1991).

Clouds, especially those containing liquid water, have long been known to be an important part of Arctic climate as a result of their effect on the surface radiation budget (e.g., Stramler et al. 2011; Shupe and Intrieri 2004). These clouds have been observed frequently at multiple Arctic locations and can persist for days (Shupe 2011; Shupe and Intrieri 2004). At Summit, they provide a positive cloud radiative forcing year-round, unlike most Arctic locations, due to Summit maintaining a high surface albedo year-round (Miller et al. 2015) and the prevalence of surface-based temperature inversions over the ice surface (Miller et al. 2013). Clouds have also been linked to both the surface melt at Summit in July 2012 (Bennartz et al. 2013; Solomon et al. 2017) and enhanced meltwater runoff across the ice sheet (Van Tricht et al. 2016). In particular, low-level liquid-bearing clouds (LBCs) with liquid water paths (LWPs) between 10 and 40 gm^{-2} were shown to be a necessary component, along with the advection of warm, moist air over the GIS, to the 2012 melt event at Summit (Bennartz et al. 2013). Within this range of LWPs, clouds can emit effectively in the infrared while still being optically thin enough to allow some solar radiation to penetrate through to the surface, thus maximizing their radiative influence on the surface. Clouds with LWP values within this range at Summit have also been found to correspond to unstable boundary layers due to the surface heating resulting from this combination of positive longwave and shortwave radiative forcing (Miller et al. 2017).

Due to their importance and the relative lack of previous study, a greater understanding of liquid cloud occurrence (especially for clouds that exist longer than 6 h and that can be considered "long lived") and properties over the GIS is warranted. Since both moisture and temperature of the atmosphere over the GIS (e.g., Mosley-Thompson et al. 2005) and precipitation over the exterior of the ice sheet (e.g., Schuenemann et al. 2009) have been linked to large-scale atmospheric patterns, here we investigate the hypothesis that the occurrence and properties of LBCs have a relationship to the large-scale atmospheric conditions.

Datasets used in this analysis will be discussed in section 2. This will be followed by a discussion of the LBC properties at Summit and the relationship between cloud occurrence/properties and the NAO in section 3. A summary of results and future work is presented in section 4.

2. Data and methods

a. ICECAPS data

Beginning in the summer of 2010, the Integrated Characterization of Energy, Clouds, Atmospheric State, and Precipitation at Summit (ICECAPS) project has collected observations of cloud, atmospheric, and precipitation properties at Summit Station, Greenland (Shupe et al. 2013). Summit is located at approximately 72°N and 321°E at an elevation of 3.2 km above sea level. The remote sensors relevant to this work are summarized below. This is followed by a discussion of non-ICECAPS datasets used herein.

1) MICROPULSE LIDAR

The micropulse lidar (MPL) is a backscatter lidar capable of sensing clouds and aerosols up to 15 km in altitude at Summit at a resolution of 15 m in the vertical and 3 s temporally (Campbell et al. 2002; Flynn et al. 2007). The MPL is polarization sensitive, alternating between transmitting horizontally and circularly polarized laser beams, which allows for the derivation of the linear depolarization ratio and total backscatter (Flynn et al. 2007). The total backscatter is proportional to the number concentration of hydrometeors and the linear depolarization ratio is strongly sensitive to the particle phase (Sassen 1991). This allows for the detection of both cloud ice and liquid water. In addition, the MPL's receiver is active before the laser activates, allowing for the sampling of the ambient radiation of the same wavelength. Using the total backscatter and the ambient measurement allows for the calculation of the signal-to-noise ratio, defined herein as the ratio of the total backscatter to the background.

2) CLOUD DETECTION

To determine the presence of a cloud, the MPL dataset is augmented with a temperature mask created using twice-daily radiosondes launched at Summit. First, clouds are identified if the signal-to-noise ratio or the total backscatter is greater than thresholds determined from manual analysis of the MPL data from Summit. Clouds identified where the temperature is less than -40°C are defined as ice and clouds identified where the temperature is greater than 0°C are defined as liquid. For clouds identified with temperatures between 0° and -40°C , liquid is defined as any point where the

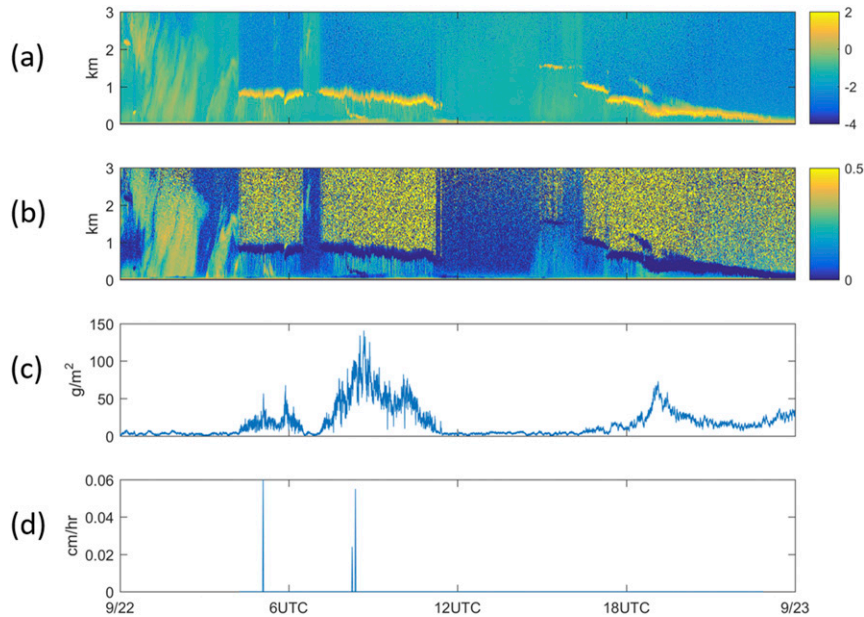


FIG. 1. ICECAPS data from 22 Sep 2013. Two LBC events were identified on this day. The first occurred from approximately 0400 to 1100 UTC, and the second occurred from approximately 1600 to 2300 UTC. Shown here are the (a) backscatter from the MPL, (b) linear depolarization ratio from the MPL, (c) LWP (g m^{-2}) retrieved from the MWRs, and (d) precipitation rate (cm h^{-1}) as observed by the POSS.

total backscatter is greater than another, more stringent, threshold and the linear depolarization ratio is less than 0.07. This is inflated slightly from the value of 0.05 used by Sassen (1991) to account for instrument uncertainties.

This cloud mask is then used to identify LBC cases. For the purposes of this analysis, a case is defined as any time when liquid is identified for at least 6 h. This length was chosen as a compromise between ensuring that cases are long lived enough to potentially have a significant, persistent effect on surface radiation and short enough so that a robust number of cases can be studied. Furthermore, for one LBC case to end and another to begin, there must be at least 3 h when no liquid is detected. Finally, to prevent spurious cases where liquid is only sporadically present, liquid must be present for at least 80% of the case lifetime. Results are not sensitive to small changes of 20% or less in the chosen thresholds.

This method was used on MPL and sounding data for the period 1 June 2010–30 September 2015, yielding 326 long-lived LBC cases, herein referred to as LBC cases for brevity. The longest-lasting 25% of cases will also be analyzed separately to determine if there are any differences when only considering this subset.

An example of ICECAPS data from 22 September 2013 consisting of two LBC cases separated by 5 h of clear skies is shown in Fig. 1. These liquid-bearing clouds appear as relatively thin regions of high backscatter

(Fig. 1a) and low depolarization ratio (Fig. 1b) measured by the MPL. The first case has a relatively constant cloud-base height of just under 1 km for the entire duration. The second case is marked by a steady decrease in altitude from around 1 km initially to near the surface by case end.

3) MICROWAVE RADIOMETERS

At Summit, two microwave radiometers (MWRs) are coupled to take measurements simultaneously at 2-s temporal resolution (Rose et al. 2005). The Humidity and Temperature Profiler measures downwelling radiance at 14 frequencies from 22 to 58 GHz. This is augmented by the high-frequency microwave radiometer, which measures downwelling radiance at 90 and 150 GHz (Turner et al. 2009). These data are used to retrieve the column-integrated liquid water path (Turner et al. 2007). Using the higher frequencies leads to lower uncertainty in the retrieval of LWP (Cadeddu et al. 2013). In addition, the retrievals of LWP at Summit utilize a model with an improved treatment of supercooled liquid water absorption (Turner et al. 2016). The use of this improved model and the utilization of higher frequencies in the retrieval led to an average uncertainty of LWP retrievals at Summit of less than 5 g m^{-2} . Data from the MWRs at Summit are available for 265 of the 326 (81%) LBC cases.

An example of MWR data for the two LBC cases discussed in section 2 shows that LWP is more highly variable for the earlier case, with values ranging from close to 0 to over 100 g m^{-2} (Fig. 1c). Both the variability and the mean value of LWP are lower for the case observed later in the period, with the maximum observed LWP only briefly peaking above 50 g m^{-2} . The observed LWP matches well with the identification of LBCs using MPL and sounding data.

4) PRECIPITATION OCCURRENCE SENSOR SYSTEM

The Precipitation Occurrence Sensor System (POSS) is a horizontally polarized X-band radar that measures the backscatter in a single near-surface sample volume (Sheppard 2007). From these data, 1-min averages of snowfall rate are derived (Sheppard and Joe 2008). Two measures of precipitation are computed for each LBC case: mean precipitation rate and precipitation fraction, defined as the fraction of measurements from the POSS during the event period with nonzero precipitation. POSS data are available for 251 of the 326 (77%) LBC cases.

POSS data from the two cases indicate very brief sporadic precipitation during the first case and zero precipitation during the second case (Fig. 1d).

b. Non-ICECAPS data

The daily NAO, Arctic Oscillation (AO), and Pacific–North America teleconnection (PNA) indices were obtained from NOAA’s Climate Prediction Center (http://www.cpc.ncep.noaa.gov/products/precip/CWlink/daily_ao_index/teleconnections.shtml). To characterize the large-scale environment during the occurrence of LBCs, the ERA-Interim reanalysis provided by the European Centre for Medium-Range Weather Forecasts is used at 0.75° grid spacing and 6-hourly temporal resolution on isobaric levels (Dee et al. 2011). Variables from ERA-Interim used herein are temperature, specific humidity, relative humidity, geopotential height, and zonal and meridional winds.

To determine the source region of air parcels arriving at Summit, backward trajectories are computed using NOAA/Air Resources Laboratory’s Hybrid Single-Particle Lagrangian Integrated Trajectory model (HYSPLIT; Stein et al. 2015; Draxler and Hess 1998). HYSPLIT trajectories use data from the Global Data Assimilation System (Kanamitsu 1989).

3. Results

a. Cloud properties

There is a pronounced late summer maximum in the number of cases of LBCs with decreases throughout each subsequent season to a minimum in spring

(Fig. 2a). The seasonality of LBC occurrence at Summit is similar to that observed at Barrow and during SHEBA for purely liquid clouds, but mixed-phase clouds at Barrow, Eureka, and SHEBA and liquid-only clouds at Eureka experience a maximum in occurrence during the fall (Shupe 2011). Most cases are relatively short lived with durations near the 6-h minimum case length, but there is a tail in the distribution with the longest cases lasting over 100 h (Fig. 2b). Most cases are low in altitude, with the height of the liquid layer often lower than 1 km above the ice sheet (Fig. 2c). This is consistent with observations of stratiform, liquid-bearing clouds from other Arctic locations (de Boer et al. 2009; Shupe 2011).

A mean liquid water path within the $10\text{--}40 \text{ g m}^{-2}$ range, which has previously been linked to surface melt at Summit specified by Bennartz et al. (2013), is observed in 59% of LBC cases (Fig. 2d). Furthermore, 41% of all LWP observations during cloud occurrence are in this range (not shown). The mean LWP at Summit during LBC occurrence is 34 g m^{-2} , which is smaller than that found at Barrow (106 g m^{-2} ; de Boer et al. 2009) and during SHEBA (61 g m^{-2} ; Shupe et al. 2006) but comparable to that at Eureka (38 g m^{-2} ; de Boer et al. 2009).

Precipitation is common, but sporadic, during the occurrence of LBCs (Fig. 2e). Only approximately 10% of cases had no precipitation measured by the POSS. However, only 10% of cases had a precipitation fraction greater than 0.5 (Fig. 2f). Both precipitation and LWP have pronounced seasonal cycles with maximum values in the summer (June–August) and minima in the spring (March–May) (Figs. 2g,h). A similar seasonal variation in precipitation was found by Castellani et al. (2015).

The seasonal cycles in LWP and precipitation are similar to the cycle in cloud occurrence. Not only are more LBC cases found in the summer, these cases also have higher mean precipitation rates and LWPs than those occurring during other seasons.

b. Large-scale atmospheric conditions

To characterize the large-scale atmosphere during the occurrence of LBCs, ERA-Interim reanalysis data are composited for all events at the time step in the ERA dataset closest to the onset of cloud occurrence. Anomalies for each case are calculated relative to the 1979–2014 monthly climatology prior to compositing. Subtracting monthly climatologies is necessary because of the disproportionate amount of events occurring during the summer. In the following analysis we composite means and anomalies of horizontal wind, relative humidity, and specific humidity at 650 hPa. This level was chosen since it is the lowest level in the ERA-Interim dataset consistently above the ground at Summit and the majority

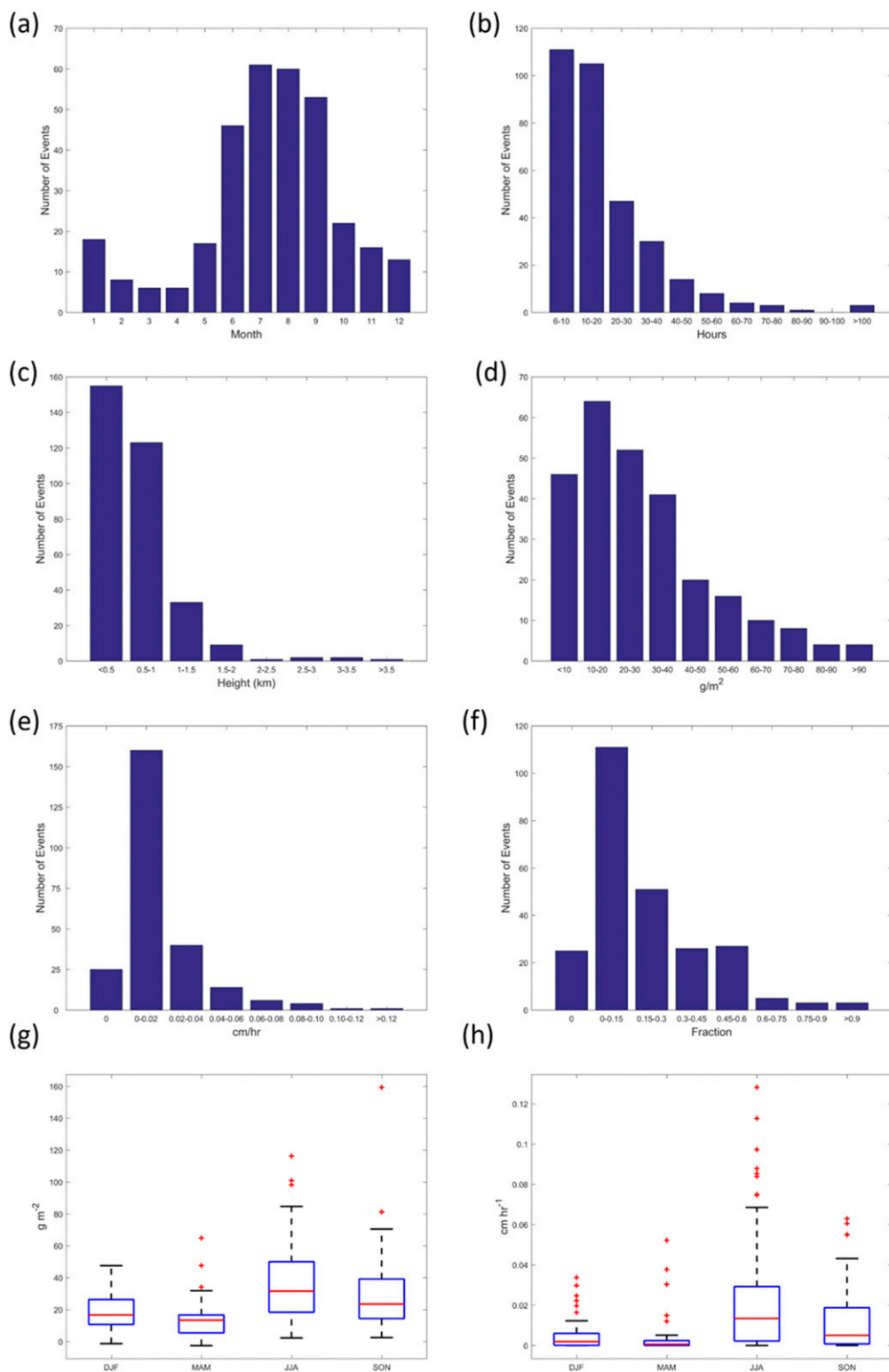


FIG. 2. Histograms of (a) event month, (b) event duration (h), (c) mean height of cloud liquid base (km), (d) mean LWP ($g\ m^{-2}$), (e) mean precipitation rate ($cm\ h^{-1}$), and (f) precipitation fraction and seasonal boxplots of (g) LWP and (h) mean precipitation rate during cloud occurrence. For the boxplots the red line is the median, the box edges are the 25th and 75th percentiles, the whiskers are the most extreme values not considered outliers, and the red plus signs are outliers.

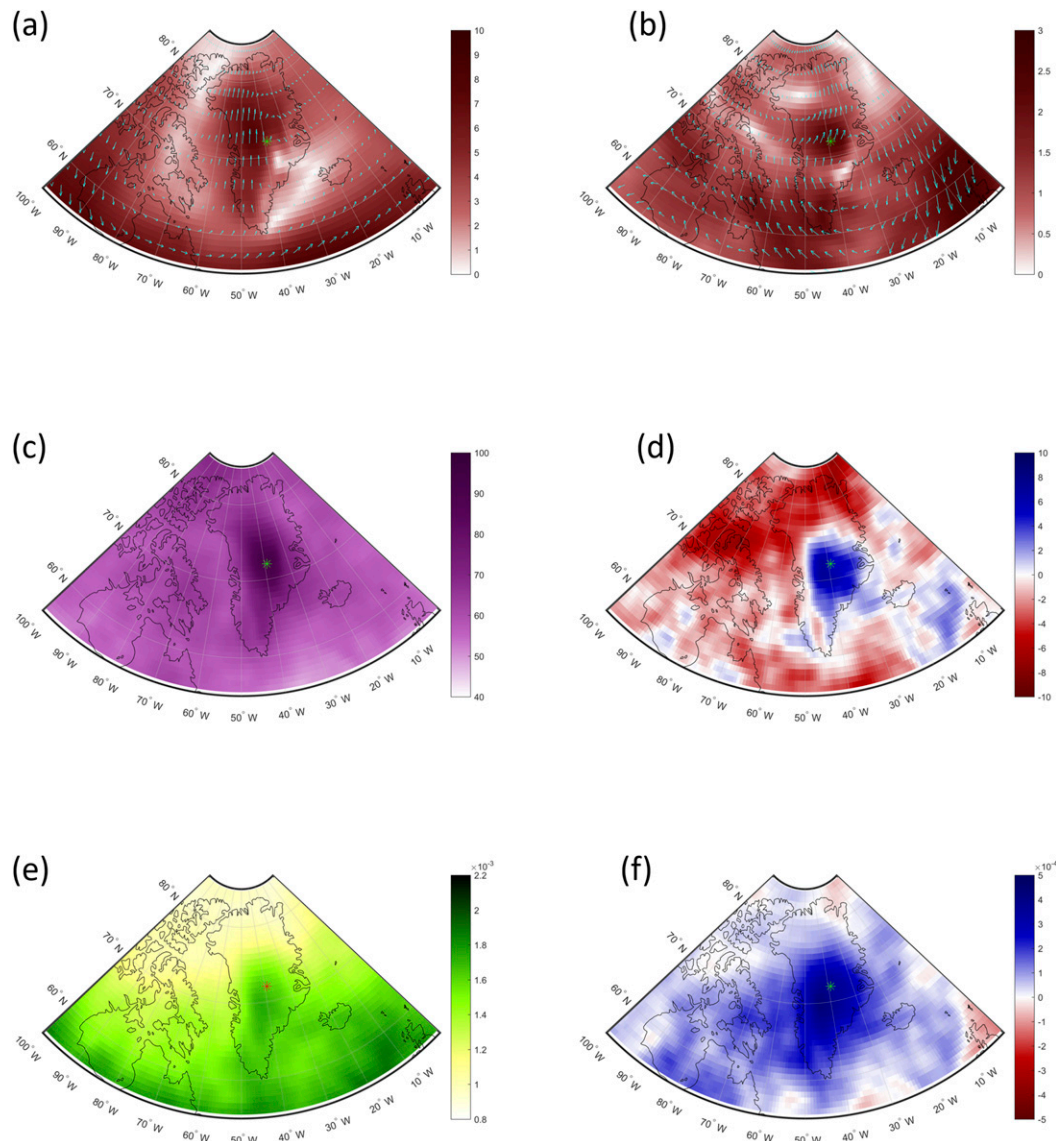


FIG. 3. Composite means of 650-hPa (a) horizontal wind (m s^{-1}), (c) relative humidity (%), and (e) specific humidity (kg kg^{-1}) for all LBC cases. Also shown are composite anomalies of 650-hPa (b) horizontal wind (vector) and the magnitude of this vector (colors) (m s^{-1}), (d) relative humidity (%), and (f) specific humidity (kg kg^{-1}) for all LBC cases at case onset. The green asterisk [red in (e)] indicates the location of Summit. The wind vectors in (a) and vector anomalies in (b) are given by the blue arrows.

of LBC cases at Summit are observed at low altitudes (see section 3a).

Southerly winds are observed over most of the GIS at the onset of LBC occurrence (Fig. 3a). These winds are anomalously strong as a result of the presence of an anticyclonic circulation anomaly centered over the eastern coast of Greenland (Fig. 3b). Analysis of data from a surface meteorology station at Summit is consistent with the ERA-Interim data with predominately south/southwesterly winds observed during LBC occurrence (not shown).

Positive relative and specific humidity anomalies are observed over the same region of the GIS experiencing anomalously strong southerly winds (Figs. 3c,d). Positive specific humidity anomalies are observed over the entire GIS, but are strongest over the central portion of the ice sheet. Relative humidity anomalies are only positive over the central GIS and are collocated with the strongest anomalies of specific humidity (Figs. 3e,f). This is due to the orographic lift of moist air parcels along the edge of the ice sheet (discussed in section 3d). The positive relative humidity anomalies are not as

spatially broad because of the widespread anomalously warm temperatures observed over much of the plotting domain (not shown).

The initial large-scale atmospheric setup does not appear to have any relationship with the duration of LBC events. Similar patterns are observed when only considering the longest-lived cases (not shown).

c. Relationship with the NAO

LBCs are observed more frequently during the $-NAO$ relative to the $+NAO$ (Fig. 4). Differences between the NAO index at LBC onset and both the distributions of the NAO climatology and NAO index during the ICECAPS period are statistically significant at the 95% confidence level using a Kolmogorov–Smirnov test. Additionally, the preference for LBC occurrence during the $-NAO$ is still found when only considering LBC cases occurring in a particular season (not shown). The disproportionate amount of LBCs during the $-NAO$ is likely related to the large-scale transport of moisture over the ice sheet noted during this phase (Mosley-Thompson et al. 2005; Bromwich et al. 1999). This is consistent with the observations of broad humidity anomalies over the GIS during LBC occurrence discussed in the previous section. The AO and the PNA pattern were also analyzed in relation to LBC occurrence (not shown). The distribution of the PNA index at event onset was not statistically different from climatology, and while the distribution of the AO index was statistically different, the magnitude of the difference was much smaller than that of the NAO.

The large-scale environmental conditions discussed in section 3b are consistent with a negative NAO pattern characterized by positive pressure anomalies over Greenland. This circulation anomaly is associated with an increase in the magnitude of the southerly-to-southwesterly winds over the ice sheet leading to moisture transport from the south. Given that LBCs are not ubiquitous during this phase of the NAO, differences in circulation patterns over Greenland during LBC occurrence in each phase are explored.

Results are similar when only considering the longest-lived 25% of LBC cases with more cases observed during the $-NAO$ as compared with the $+NAO$.

To assess the flow patterns during LBC cases occurring in each phase of the NAO, positive and negative NAO cases are defined herein as cases occurring when the NAO index is greater (less) than 0.5 (-0.5) at case onset. This threshold was reduced from the typical ± 1 standard deviation used in the literature due to the small number of LBC events occurring during the $+NAO$. This yields 46 (145) positive (negative) cases. During this subset of $-NAO$ cases, the expected ridging pattern

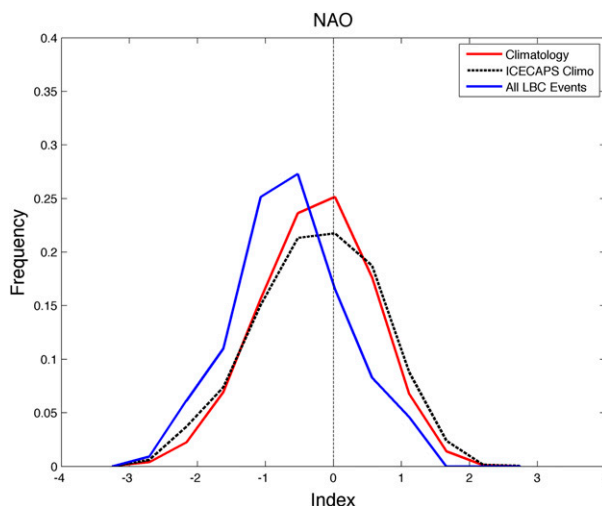


FIG. 4. Probability density function of the NAO index at case onset (blue), the 1979–2014 climatology of the NAO (red), and the climatology of the NAO during the ICECAPS period (black dashed).

yielding southwesterly flow over the ice sheet is observed (Fig. 5a). However, during the subset of $+NAO$ cases a low pressure center is located off the southeastern coast of the ice sheet (Fig. 5b). This pattern is frequently observed when plotting geopotential height at the onset of individual LBC events (not shown). Cyclonic flow wrapping around a low pressure center located in this region could potentially lead to southeasterly-to-easterly flow at Summit. Low pressure systems in this area have previously been linked to precipitation along the periphery of the ice sheet (Schuenemann et al. 2009). This precipitation is linked to the interaction of cyclonic circulation impacting the topography of the GIS.

To further explore the origin of air parcels that arrive at Summit during LBC occurrence, HYSPLIT backward trajectories are computed at case onset. Trajectories are initialized at the first hour after case onset and at mean cloud-base height for the case. Each backward trajectory is run for 72 h, the longest option available in HYSPLIT. From these data, the source location (where the air parcels are first located over the ice sheet) is defined as the location of the parcel at -72 h unless one of the following two conditions is met: 1) the parcel reaches the ground (this was considered unphysical), in which case the trajectory data after this point are discarded, making the end of the trajectory earlier than -72 h, or 2) the parcel leaves the ice sheet (defined as the first time the terrain height in HYSPLIT is equal to 0, meaning the parcel is located over the ocean). The source locations of air parcels match the inferred locations from the patterns in geopotential height outlined

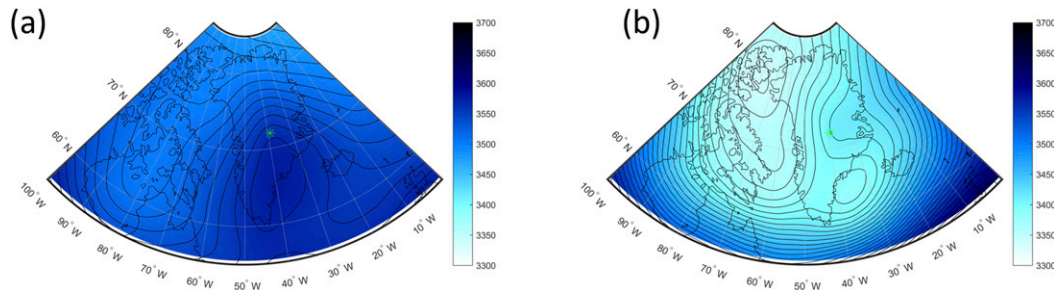


FIG. 5. Geopotential height (m) composites at case start for LBCs initiating when (a) the NAO index is less than -0.5 and (b) the NAO index is greater than 0.5 .

above (Fig. 6a). During the +NAO, parcels first reach the ice sheet along the southeast coast (Fig. 6d), while during the -NAO the parcels first reach the ice sheet along the southwest coast (Fig. 6f). It should be noted that while most parcels first reach the ice sheet from the southwest during the -NAO, some parcels first reach the ice sheet from the southeast. This is potentially due to the presence of either a closed high over the GIS leading to anticyclonic circulation of parcels around the ice sheet or ridging, which is not centered over the central GIS.

Since the LBCs observed at Summit come from two separate large-scale situations, a natural question is: are the mean microphysical properties of clouds occurring in each situation similar or different? Table 1 lists the mean and standard deviation of all LWP and precipitation-rate observations during +NAO and -NAO cases. The mean LWP is approximately 15 g m^{-2} higher during the -NAO cases than in the +NAO cases. In addition, the correlation coefficient between event mean LWP and the daily NAO index at event onset is -0.21 with a p value of 7.1×10^{-4} . LWP is also more variable during the -NAO with a correlation of -0.16 between event LWP standard deviation and the daily NAO index with a p value of 0.09 . A possible explanation for the lower average LWP during the +NAO is that the origin of the air parcels that arrive at Summit is from locations close to the low pressure systems, where ascent is favored during this phase. Since ascent is favored both around low pressure systems and at the periphery of the ice sheet because of orography, much of the atmospheric moisture could be condensed and precipitated out prior to the air reaching Summit. Conversely, during the -NAO, ascent is not favored before air parcels reach the edge of the ice sheet because of the presence of a ridge. This simplified moisture transport could also partly explain the increased number of LBC cases during the -NAO. Analysis of the precipitation rate along HYSPLIT trajectories provides support for this theory. Precipitation is more common and heavier

along the backward trajectories for the +NAO cases as compared with the -NAO cases.

Additionally, the smaller mean LWP value during the +NAO events (Table 1) is more centered in the LWP range specified by Bennartz et al. (2013) and Miller et al. (2017) that leads to maximum downwelling total radiative forcing (longwave plus shortwave) at the surface at Summit (relative to the mean LWP in -NAO events). This is also evident when considering all LWP observations in the two categories (Fig. 7a). LWP observations less than approximately 40 g m^{-2} are more common during the +NAO, while observations of LWP greater than 40 g m^{-2} are more common during the -NAO. This difference in LWP between the two phases can result in significantly different radiative heating rate profiles within and around the cloud as shown by Turner et al. (2018), who demonstrated that both shortwave and longwave radiative heating-cooling rate profiles of Arctic clouds are dependent on LWP. Shortwave radiation results in primarily warming throughout LBCs while longwave emission results in cooling; however, the longwave and shortwave heating rate profiles have different structures in the cloud. In addition, the longwave cooling is approximately 3–5 times greater in magnitude than the shortwave heating. These differences in the total radiative heating rate profiles in these clouds, due to the characteristic differences in the mean LWP for +NAO and NAO events, can result in different dynamical feedbacks in the two categories of clouds because of the importance of radiation in maintaining LBCs (Solomon et al. 2017; Morrison et al. 2012).

In contrast to LWP, the event mean and standard deviation of the precipitation rate do not have statistically significant correlations to the NAO index. However, when looking at all precipitation-rate observations during +NAO and -NAO events, there is a difference in the distributions. Precipitation rates of 0 cm h^{-1} constitute 74% of all observations during -NAO cases and 83% of all observations during +NAO cases and nonzero precipitation rates are more common during

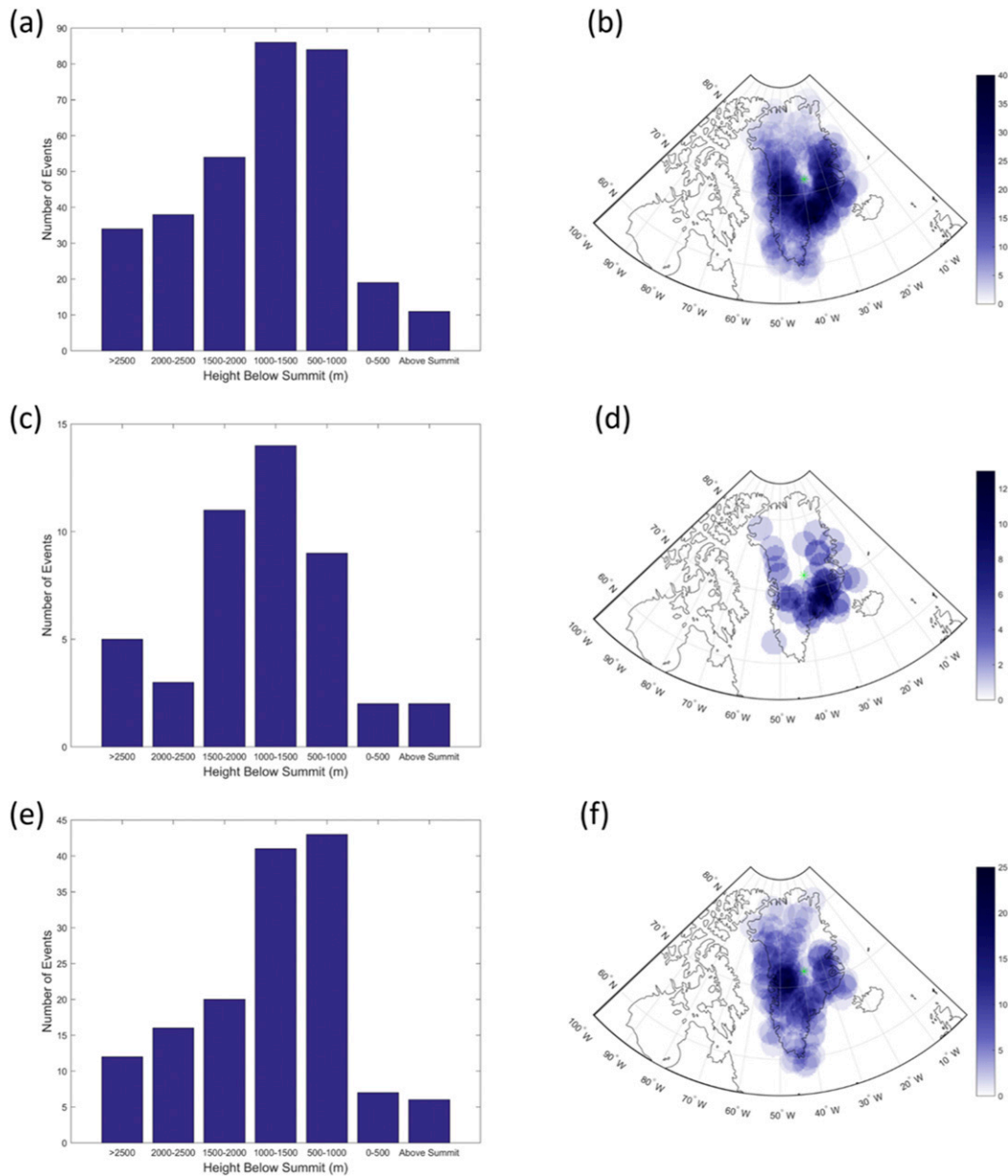


FIG. 6. The minimum height, relative to Summit, between trajectory initialization and source location for (a) all LBC events, (c) events occurring during the +NAO, and (e) events occurring during the -NAO. Also shown is the number of parcels sourced from within 200 km of a point in HYSPLIT for (b) all LBC events, (d) events occurring during the +NAO, and (f) events occurring during the -NAO.

the -NAO (Fig. 7b). This has implications for the surface mass budget of the GIS. A greater positive impact on the surface mass budget, due to accumulation, is attributable to LBCs occurring during the -NAO. The decreased precipitation rate could also be explained by the same logic as the variations in LWP with the NAO (i.e., more moisture is lost during +NAO events due to ascent prior to air parcels reaching Summit). This synoptic setup during +NAO events is similar to cold-air

damming events along the Colorado Front Range, where low-level upslope flow can be induced by the presence of a surface cyclone to the south (e.g., Dunn 1987). Cold-air damming events in this region can lead to heavy snowfall along the slope of the mountains (Dunn 1987). Similarly, precipitation along the edge of the GIS has been linked to the interaction between cyclones and the steep terrain along the edge of the ice sheet (Schuenemann et al. 2009).

TABLE 1. Microphysical cloud properties for +NAO and -NAO LBC cases.

Cloud microphysical property	+NAO cases	-NAO cases
Mean LWP (g m^{-2})	20.36	35.82
Std dev of LWP (g m^{-2})	23.24	37.99
Mean precipitation rate (cm h^{-1})	0.013	0.020
Std dev of precipitation rate (cm h^{-1})	0.044	0.051

Orographic effects will be discussed further in the next section.

d. Orographic lift

Given previous research indicating the importance of orographic lift on precipitation in Greenland and the fact that air parcels must pass over the steep terrain on the edge of the ice sheet in order to reach Summit, we are interested to explore the potential role orographic lift plays in the occurrence of LBCs. In HYPPLIT, the minimum height relative to the model height of Summit was computed for each case. This computation only considered the portion of the backward trajectories between initialization and source location (as defined in the previous section). The results for each group are similar with most parcels originating from elevations well below Summit. The distributions peak around a height change of 1–2 km; this indicates that most parcels originate 1–2 km below the altitude of Summit and thus about 1–2 km above the mean sea level (Fig. 6). For only 11 of the 326 cases did the parcels remain above the altitude of Summit for their entire trajectory.

Initially, the strongest anomalies in specific humidity are found to the south of the ice sheet at elevations below the height of Summit (Figs. 8a–c). However, by the onset of LBC occurrence, the anomalies at the top of the ice sheet have increased in magnitude and are comparable to the anomalies to the south at lower elevations. This indicates that moisture at Summit during LBC occurrence is, at least in part, originating from below the elevation of Summit. Throughout the same period, mean southerly winds are observed, which are anomalously strong throughout most of the troposphere (not shown).

To further investigate this, the Froude number Fr is computed using data from the ERA-Interim reanalysis interpolated onto a constant height grid as follows:

$$Fr = \frac{U}{NH}, \quad (1)$$

where U is the magnitude of the wind speed at the analysis level, H is the height from the analysis level to Summit, and N is the Brunt–Väisälä frequency. Since the reanalysis data are interpolated onto a constant

height grid, H is constant at any given analysis level. The value of N is calculated as follows:

$$N = \left(\frac{g}{\bar{\theta}} \frac{\partial \theta}{\partial z} \right)^{1/2}, \quad (2)$$

where g is the acceleration due to gravity, $\bar{\theta}$ is the average potential temperature in the layer from the analysis level to Summit, and $\partial \theta / \partial z$ is the change in potential temperature with height in the layer.

The Froude number can be interpreted as being proportional to the ratio of the kinetic energy (which is proportional to U) to the stability of the environment between a point below a barrier of height H to the top of the barrier (NH). When the Froude number exceeds 1, the kinetic energy (wind speed) is high enough to overcome atmospheric stability and allow an air parcel to pass over a barrier of height H (e.g., Markowski and Richardson 2011).

To evaluate how flow patterns are different during the occurrence of LBCs as compared with the ICECAPS period as a whole, the Froude number is computed at every time and point when the winds are $\pm 45^\circ$ from the analysis point to Summit for the period 1 June 2010–30 September 2015, the period during which LBC cases were identified. The $\pm 45^\circ$ bounds are enforced to remove times when the wind is not impacting the terrain of the ice sheet. The percent of LBC cases that meet this criterion at a height of 2750 m for the onset of cloud occurrence is shown in Fig. 9. A height of 2750 m was chosen since the mean value of Fr was close to 1 at this level around much of the ice sheet. Moving up to 3000 m results in values of Fr well above 1 surrounding the ice sheet, while moving down to 2500 m results in Fr values less than one over the majority of the plotting domain. As expected, winds are within the $\pm 45^\circ$ bound most frequently for grid points along the southwest slope of the ice sheet where southwesterly flow is commonly observed during the -NAO. For +NAO cases (Fig. 9b), the eastern coast of the ice sheet is highlighted as well because of the flow from cyclones passing along the coast as discussed in the previous section while during -NAO cases (Fig. 9c) only the southwestern coast is highlighted.

At times when the wind direction is within the specified bounds, the mean Froude number is near or greater than one at all points around the southeastern and southwestern edges of the ice sheet, indicating that air parcels are favored to reach the top of the ice sheet from an elevation of 2750 m (Fig. 10a). In addition, the Froude number at LBC onset is greater than the ICECAPS climatology over the same area (Fig. 10b). The statistical significance of these anomalies was tested using a two-tailed z test. Nearly all of the anomalies over the southwestern, southern, and southeastern coasts of

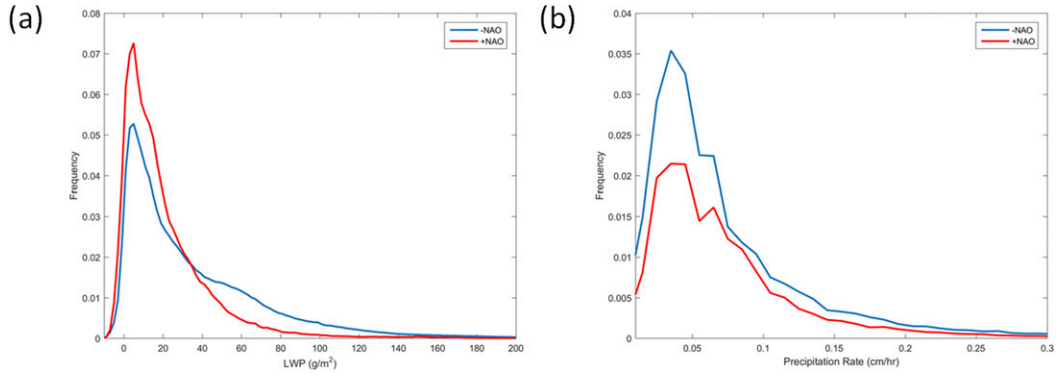


FIG. 7. Probability density functions of (a) LWP (g m^{-2}) and (b) precipitation-rate (cm h^{-1}) observations during positive (red) and negative (blue) NAO events. Precipitation-rate observations of 0 are not shown here. Approximately 74% of precipitation-rate observations during the $-$ NAO are 0 as compared with approximately 83% during the $+$ NAO.

the ice sheet are found to be statistically significant at the 95% confidence level.

To better isolate the reason behind the increased Froude number, the numerator U and denominator NH

of the Froude number calculation were computed separately for the entire ICECAPS period. Since computations are performed on data with height as the vertical coordinate, comparing changes in dynamics and stability

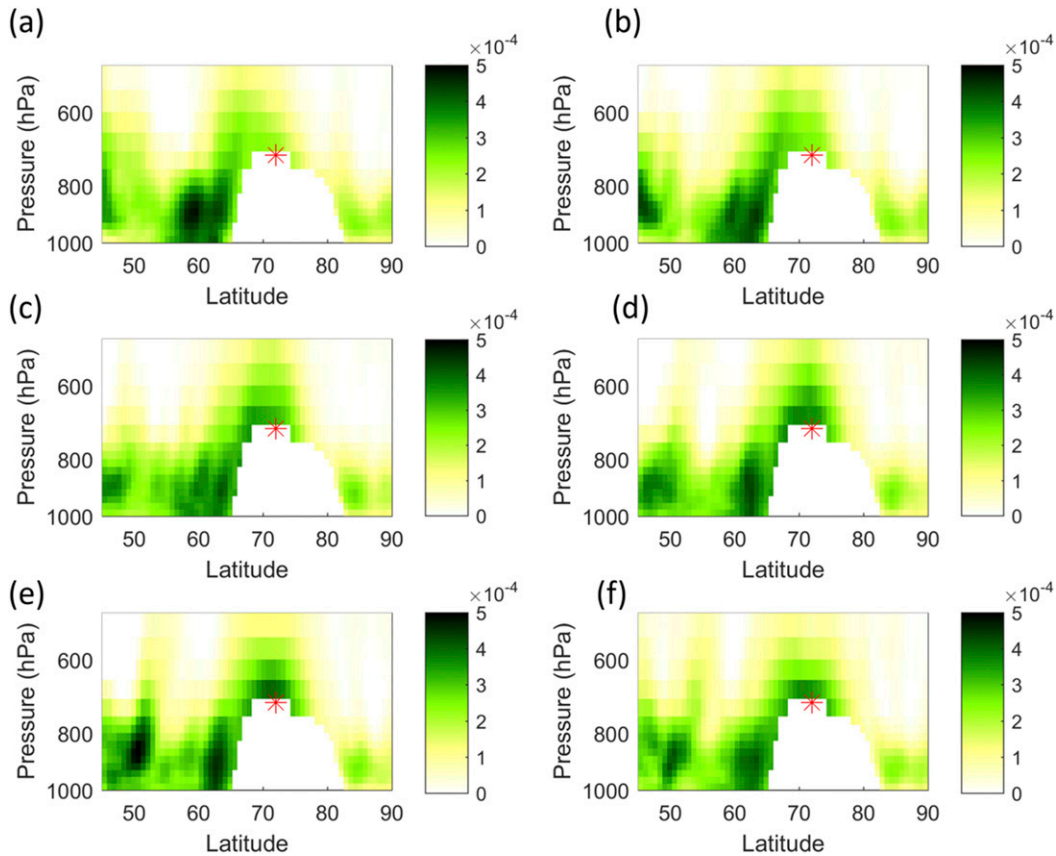


FIG. 8. Meridional cross sections of specific humidity anomalies (kg kg^{-1}) (a) 18, (b) 12, and (c) 6 h prior to case start, (d) at case start, and (e) 6 and (f) 12 h after case start along the longitude of Summit. The red asterisk indicates the location of Summit. The cross sections are at 321.25° and are averaged across ± 1 longitude grid step.

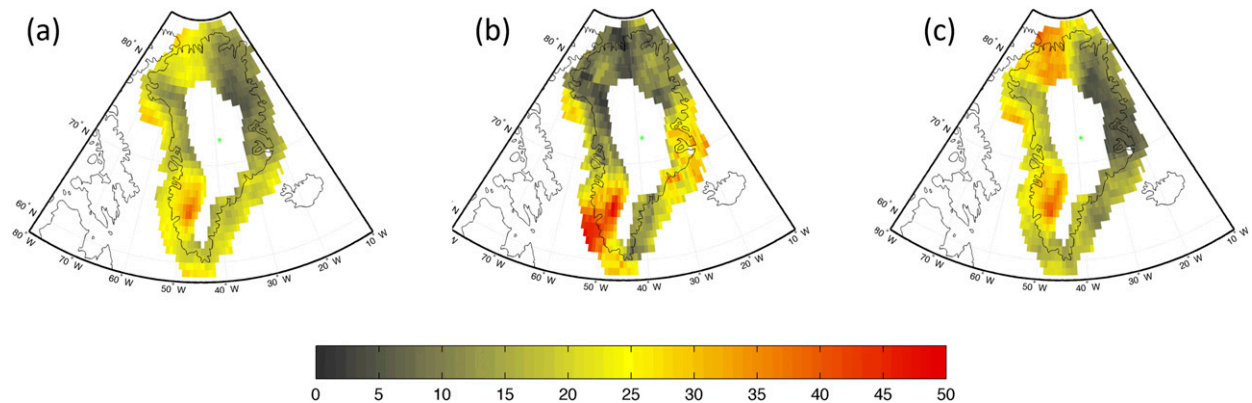


FIG. 9. Percent of LBC cases with wind directions $\pm 45^\circ$ from Summit for (a) all cases, (b) +NAO cases, and (c) -NAO cases.

is significantly simplified. Both U and NH have units of meters per second, and since H is constant, any variations in the denominator are solely due to changes in the Brunt–Väisälä frequency (i.e., stability). There are statistically significant increases in U around much of the ice sheet (Figs. 10c,d). These anomalies have a very similar spatial pattern to those of the full Froude number. In contrast, anomalies of NH are much smaller and not statistically significant around much of the southern portion of the ice sheet (Figs. 10e,f). This indicates that the increases in the Froude number at LBC onset are primarily due to anomalously strong horizontal winds in an environment with close to average stability.

This is consistent with the results from HYSPLIT, which also indicated that parcels were rising from elevations below Summit at cloud onset. There is one notable difference between the Froude number and the HYSPLIT results. While the results from HYSPLIT indicate that parcels are often rising from elevations of 1–2 km above sea level, analysis of the Froude number at different levels indicates that parcels are rising from elevations closer to 2.5 km. This is potentially due to assumptions with the Froude number calculation—namely the lack of consideration paid to atmospheric moisture and its impact on stability. While there are differences, it should be noted that both methods still indicate that air is being lifted by the terrain of the ice sheet.

4. Discussion

LBCs have a significant radiative impact on the surface across the Arctic (e.g., Shupe 2011). Given the importance of understanding their occurrence and previous research indicating the importance of the NAO (e.g., Mosley-Thompson et al. 2005) and low pressure systems interacting with the steep terrain of the ice sheet (Schuenemann et al. 2009) to Greenland’s climate, the

relationship between the large-scale atmosphere and LBCs occurring at Summit was explored.

In this study, data from the ICECAPS program were used to diagnose the occurrence of LBCs over the GIS. There is a maximum in occurrence during the summer and a minimum in the spring. A similar cycle in mean precipitation rate and mean LWP is observed, with maxima in both variables observed during summer LBC cases. LWP values between 10 and 40 g m^{-2} , previously linked to the melt of the ice sheet at Summit, are frequently observed in clouds over Summit.

LBCs occurring during two atmospheric states (\pm NAO) were examined in this study and differences in both cloud occurrence and properties were observed. LBCs occurred more frequently during the -NAO. Additionally, these clouds had higher values of LWP and produced more precipitation than those occurring during the +NAO. This clearly shows the importance of the large-scale atmospheric setup to the occurrence and properties of LBCs at Summit.

During +NAO cases, air parcels at Summit originate from low pressure systems located off of the southeastern coast of Greenland. These air parcels have likely experienced ascent in the cyclone before they reach the ice sheet, potentially allowing for condensation and precipitation before the air can reach Summit and thus decreasing the observed LWP and precipitation rate in these cases. The smaller number of LBC cases observed during this phase could also be related to the relative difficulty in lifting sufficient moisture to the top of the ice sheet during the +NAO. This has implications for both the surface radiative and mass budgets at Summit. Low liquid water path clouds, like those observed during the +NAO, provide a greater positive radiative forcing to the surface of the ice sheet (Bennartz et al. 2013; Miller et al. 2017) while the greater precipitation rates observed during the -NAO provide a larger contribution for the surface mass budget.

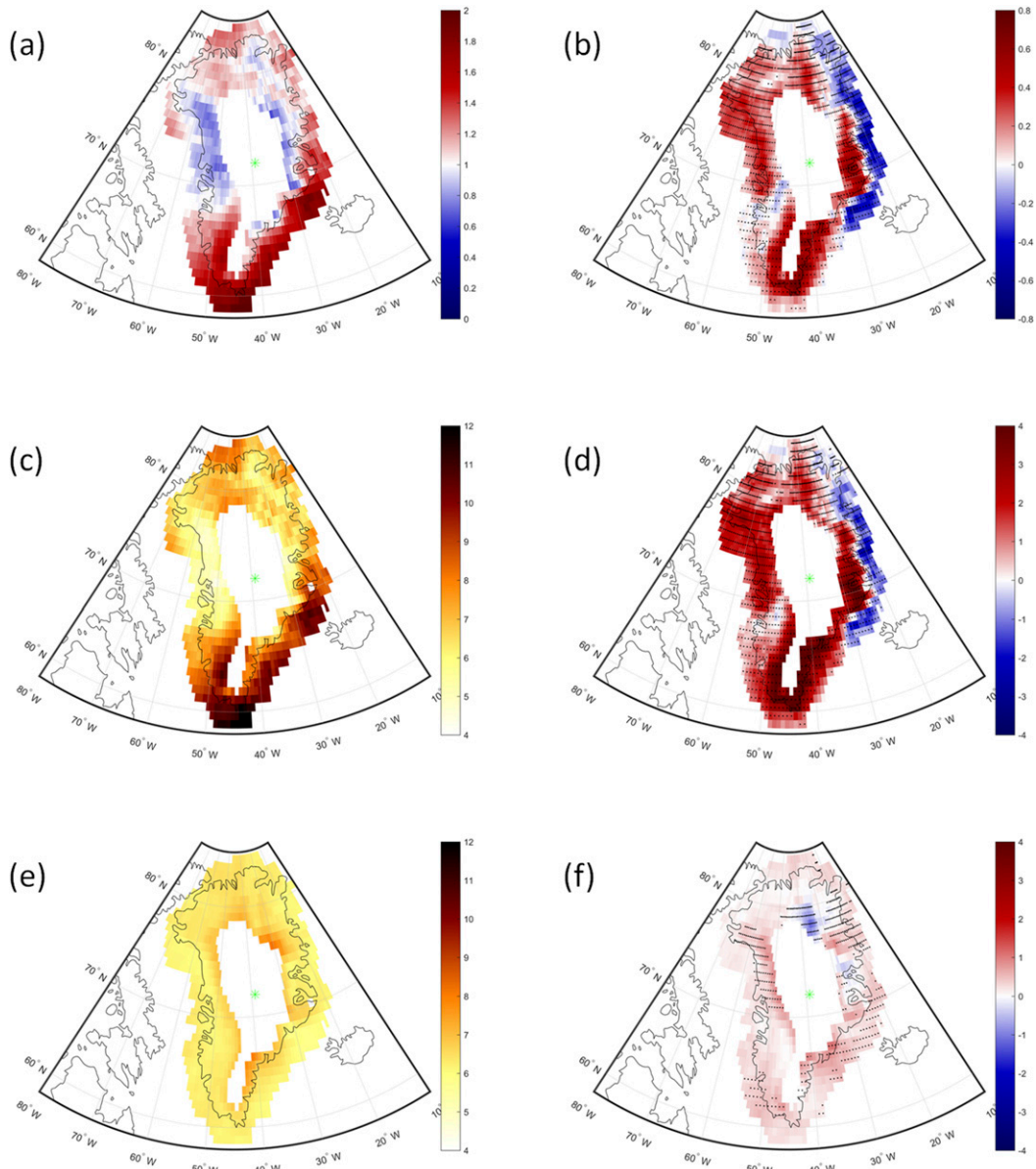


FIG. 10. (left) Mean and (right) anomalies of (a),(b) Froude number, (c),(d) U , and (e),(f) NH during the ICECAPS period. These values are only computed for times when the wind direction is $\pm 45^\circ$ from Summit (see Fig. 9). Statistically significant (95% confidence for a two-tailed z test) anomalies are indicated by black dots.

Both backward trajectories from HYSPLIT and analysis of the Froude number indicate that air parcels arriving at Summit during the occurrence of LBCs are favored to rise from altitudes below Summit, thus allowing more moist air from lower altitudes to reach the top of the ice sheet. This is likely due to increases in wind speed near the edge of the ice sheet. This increased wind speed gives parcels sufficient energy to rise over the steep terrain of the ice sheet through an atmospheric layer with close to average stability.

The effect of a warming climate on the occurrence of LBCs and the large-scale atmospheric patterns over the GIS needs to be investigated. Any changes in the properties of LBCs could impact the surface radiative and mass budgets over the ice sheet and thus impact surface melting and therefore sea level rise and the AMOC.

This work could be expanded in the future to explore differences in the results when looking at liquid-only or mixed-phase clouds separately. In addition, the seasonal cycles of LBC occurrence, LWP, and precipitation rate

observed here are not symmetric around the summer; many more cases are observed in the fall as compared with the spring and LWP and the precipitation rate are higher during these fall cases. More research is needed to fully understand the seasonal variability of both cloud occurrence and properties. In addition, further investigation is needed to explore the meteorological factors relating to the duration of the LBCs at Summit. To this point, no significant differences in large-scale atmospheric properties have been noted when only considering particularly long-lived cases. These cases could be associated with a blocking pattern and thus the persistence of the atmospheric conditions discussed in section 3b but more work investigating the time evolution of these atmospheric patterns in relation to LBC occurrence is needed to determine if this is the case.

Acknowledgments. We thank Jeff Thayer, Robert Stillwell, and Connor Flynn for discussions regarding the analysis of the MPL dataset. We thank all of the researchers, technicians, and staff involved with the ICECAPS project and, especially, those involved with the Polar Field Services that operate the site and maintain the ICECAPS instruments year-round. Additionally, we thank the students and faculty in the Arctic and Antarctic Atmospheric Research Group at the University of Oklahoma. This research was supported by the National Science Foundation via Grants 1304692 and 1314358.

REFERENCES

- Bennartz, R., and Coauthors, 2013: July 2012 Greenland melt extent enhanced by low-level liquid clouds. *Nature*, **496**, 83–86, <https://doi.org/10.1038/nature12002>.
- Bromwich, D. H., Q.-S. Chen, Y. Li, and R. I. Cullather, 1999: Precipitation over Greenland and its relation to the North Atlantic oscillation. *J. Geophys. Res.*, **104**, 22 103–22 115, <https://doi.org/10.1029/1999JD900373>.
- Cadeddu, M., J. Liljegren, and D. Turner, 2013: The Atmospheric Radiation Measurement (ARM) program network of microwave radiometers: Instrumentation, data, and retrievals. *Atmos. Meas. Tech.*, **6**, 2359–2372, <https://doi.org/10.5194/amt-6-2359-2013>.
- Campbell, J. R., D. L. Hlavka, E. J. Welton, C. J. Flynn, D. D. Turner, J. D. Spinhirne, V. S. Scott III, and I. Hwang, 2002: Full-time, eye-safe cloud and aerosol lidar observation at Atmospheric Radiation Measurement program sites: Instruments and data processing. *J. Atmos. Oceanic Technol.*, **19**, 431–442, [https://doi.org/10.1175/1520-0426\(2002\)019<0431:FTESCA>2.0.CO;2](https://doi.org/10.1175/1520-0426(2002)019<0431:FTESCA>2.0.CO;2).
- Castellani, B. B., M. D. Shupe, D. R. Hudak, and B. E. Sheppard, 2015: The annual cycle of snowfall at Summit, Greenland. *J. Geophys. Res. Atmos.*, **120**, 6654–6668, <https://doi.org/10.1002/2015JD023072>.
- de Boer, G., E. W. Eloranta, and M. D. Shupe, 2009: Arctic mixed-phase stratiform cloud properties from multiple years of surface-based measurements at two high-latitude locations. *J. Atmos. Sci.*, **66**, 2874–2887, <https://doi.org/10.1175/2009JAS3029.1>.
- Dee, D., and Coauthors, 2011: The ERA-Interim reanalysis: Configuration and performance of the data assimilation system. *Quart. J. Roy. Meteor. Soc.*, **137**, 553–597, <https://doi.org/10.1002/qj.828>.
- Draxler, R. R., and G. Hess, 1998: An overview of the HYSPLIT_4 modelling system for trajectories. *Aust. Meteor. Mag.*, **47**, 295–308.
- Dunn, L., 1987: Cold air damming by the Front Range of the Colorado Rockies and its relationship to locally heavy snows. *Wea. Forecasting*, **2**, 177–189, [https://doi.org/10.1175/1520-0434\(1987\)002<0177:CADBTF>2.0.CO;2](https://doi.org/10.1175/1520-0434(1987)002<0177:CADBTF>2.0.CO;2).
- Flynn, C. J., A. Mendoza, Y. Zheng, and S. Mathur, 2007: Novel polarization-sensitive micropulse lidar measurement technique. *Opt. Express*, **15**, 2785–2790, <https://doi.org/10.1364/OE.15.002785>.
- Kanamitsu, M., 1989: Description of the NMC Global Data Assimilation and Forecast System. *Wea. Forecasting*, **4**, 335–342, [https://doi.org/10.1175/1520-0434\(1989\)004<0335:DOTNGD>2.0.CO;2](https://doi.org/10.1175/1520-0434(1989)004<0335:DOTNGD>2.0.CO;2).
- Markowski, P., and Y. Richardson, 2011: *Mesoscale Meteorology in Midlatitudes*. John Wiley and Sons, 450 pp.
- Miller, N. B., D. D. Turner, R. Bennartz, M. D. Shupe, M. S. Kulie, M. P. Cadeddu, and V. P. Walden, 2013: Surface-based inversions above central Greenland. *J. Geophys. Res. Atmos.*, **118**, 495–506, <https://doi.org/10.1029/2012JD018867>.
- , M. D. Shupe, C. J. Cox, V. P. Walden, D. D. Turner, and K. Steffen, 2015: Cloud radiative forcing at Summit, Greenland. *J. Climate*, **28**, 6267–6280, <https://doi.org/10.1175/JCLI-D-15-0076.1>.
- , —, —, D. Noone, P. O. G. Persson, and S. Konrad, 2017: Surface energy budget responses to radiative forcing at Summit, Greenland. *Cryosphere*, **11**, 497, <https://doi.org/10.5194/tc-11-497-2017>.
- Morrison, H., G. de Boer, G. Feingold, J. Harrington, M. D. Shupe, and K. Sulia, 2012: Resilience of persistent Arctic mixed-phase clouds. *Nat. Geosci.*, **5**, 11–17, <https://doi.org/10.1038/ngeo1332>.
- Mosley-Thompson, E., C. Readinger, P. Craigmille, L. Thompson, and C. Calder, 2005: Regional sensitivity of Greenland precipitation to NAO variability. *Geophys. Res. Lett.*, **32**, L24707, <https://doi.org/10.1029/2005GL024776>.
- Ohmura, A., and N. Reeh, 1991: New precipitation and accumulation maps for Greenland. *J. Glaciol.*, **37**, 140–148, <https://doi.org/10.1017/S0022143000042891>.
- Rahmstorf, S., G. Feulner, M. E. Mann, A. Robinson, S. Rutherford, and E. J. Schaffernicht, 2015: Exceptional twentieth-century slowdown in Atlantic Ocean overturning circulation. *Nat. Climate Change*, **5**, 475–480, <https://doi.org/10.1038/nclimate2554>.
- Rose, T., S. Crewell, U. Löhnert, and C. Simmer, 2005: A network suitable microwave radiometer for operational monitoring of the cloudy atmosphere. *Atmos. Res.*, **75**, 183–200, <https://doi.org/10.1016/j.atmosres.2004.12.005>.
- Sassen, K., 1991: The polarization lidar technique for cloud research: A review and current assessment. *Bull. Amer. Meteor. Soc.*, **72**, 1848–1866, [https://doi.org/10.1175/1520-0477\(1991\)072<1848:TPLTFC>2.0.CO;2](https://doi.org/10.1175/1520-0477(1991)072<1848:TPLTFC>2.0.CO;2).
- Schuenemann, K. C., and J. J. Cassano, 2009: Changes in synoptic weather patterns and Greenland precipitation in the 20th and 21st centuries: 1. Evaluation of late 20th century simulations from IPCC models. *J. Geophys. Res.*, **114**, D20113, <https://doi.org/10.1029/2009JD011705>.

- , —, and J. Finnis, 2009: Synoptic forcing of precipitation over Greenland: Climatology for 1961–99. *J. Hydrometeorol.*, **10**, 60–78, <https://doi.org/10.1175/2008JHM1014.1>.
- Serreze, M. C., and R. G. Barry, 2011: Processes and impacts of Arctic amplification: A research synthesis. *Global Planet. Change*, **77**, 85–96, <https://doi.org/10.1016/j.gloplacha.2011.03.004>.
- Shepherd, A., and Coauthors, 2012: A reconciled estimate of ice-sheet mass balance. *Science*, **338**, 1183–1189, <https://doi.org/10.1126/science.1228102>.
- Sheppard, B., 2007: Sampling errors in the measurement of rainfall parameters using the Precipitation Occurrence Sensor System (POSS). *J. Atmos. Oceanic Technol.*, **24**, 125–140, <https://doi.org/10.1175/JTECH1956.1>.
- , and P. Joe, 2008: Performance of the Precipitation Occurrence Sensor System as a precipitation gauge. *J. Atmos. Oceanic Technol.*, **25**, 196–212, <https://doi.org/10.1175/2007JTECHA957.1>.
- Shupe, M. D., 2011: Clouds at Arctic atmospheric observatories. Part II: Thermodynamic phase characteristics. *J. Appl. Meteor. Climatol.*, **50**, 645–661, <https://doi.org/10.1175/2010JAMC2468.1>.
- , and J. M. Intrieri, 2004: Cloud radiative forcing of the Arctic surface: The influence of cloud properties, surface albedo, and solar zenith angle. *J. Climate*, **17**, 616–628, [https://doi.org/10.1175/1520-0442\(2004\)017<0616:CRFOTA>2.0.CO;2](https://doi.org/10.1175/1520-0442(2004)017<0616:CRFOTA>2.0.CO;2).
- , S. Y. Matrosov, and T. Uttal, 2006: Arctic mixed-phase cloud properties derived from surface-based sensors at SHEBA. *J. Atmos. Sci.*, **63**, 697–711, <https://doi.org/10.1175/JAS3659.1>.
- , and Coauthors, 2013: High and dry: New observations of tropospheric and cloud properties above the Greenland Ice Sheet. *Bull. Amer. Meteor. Soc.*, **94**, 169–186, <https://doi.org/10.1175/BAMS-D-11-00249.1>.
- Solomon, A., M. D. Shupe, and N. B. Miller, 2017: Cloud–atmospheric boundary layer–surface interactions on the Greenland Ice Sheet during the July 2012 extreme melt event. *J. Climate*, **30**, 3237–3252, <https://doi.org/10.1175/JCLI-D-16-0071.1>.
- Stein, A., R. Draxler, G. Rolph, B. Stunder, M. Cohen, and F. Ngan, 2015: NOAA’s HYSPLIT atmospheric transport and dispersion modeling system. *Bull. Amer. Meteor. Soc.*, **96**, 2059–2077, <https://doi.org/10.1175/BAMS-D-14-00110.1>.
- Stramler, K., A. D. Del Genio, and W. B. Rossow, 2011: Synoptically driven Arctic winter states. *J. Climate*, **24**, 1747–1762, <https://doi.org/10.1175/2010JCLI3817.1>.
- Turner, D. D., S. A. Clough, J. C. Liljegren, E. E. Clothiaux, K. E. Cady-Pereira, and K. L. Gaustad, 2007: Retrieving liquid water path and precipitable water vapor from the Atmospheric Radiation Measurement (ARM) microwave radiometers. *IEEE Trans. Geosci. Remote Sens.*, **45**, 3680–3690, <https://doi.org/10.1109/TGRS.2007.903703>.
- , M. P. Cadeddu, U. Lohner, S. Crewell, and A. M. Vogelmann, 2009: Modifications to the water vapor continuum in the microwave suggested by ground-based 150-GHz observations. *IEEE Trans. Geosci. Remote Sens.*, **47**, 3326–3337, <https://doi.org/10.1109/TGRS.2009.2022262>.
- , S. Kneifel, and M. P. Cadeddu, 2016: An improved liquid water absorption model at microwave frequencies for supercooled liquid water clouds. *J. Atmos. Oceanic Technol.*, **33**, 33–44, <https://doi.org/10.1175/JTECH-D-15-0074.1>.
- , M. D. Shupe, and A. B. Zwink, 2018: Characteristic atmospheric radiative heating rate profiles in Arctic clouds as observed at Barrow, Alaska. *J. Appl. Meteor. Climatol.*, <https://doi.org/10.1175/JAMC-D-17-0252.1>, in press.
- Van Loon, H., and J. C. Rogers, 1978: The seesaw in winter temperatures between Greenland and northern Europe. Part I: General description. *Mon. Wea. Rev.*, **106**, 296–310, [https://doi.org/10.1175/1520-0493\(1978\)106<0296:TSIWTB>2.0.CO;2](https://doi.org/10.1175/1520-0493(1978)106<0296:TSIWTB>2.0.CO;2).
- Van Tricht, K., and Coauthors, 2016: Clouds enhance Greenland Ice Sheet meltwater runoff. *Nat. Commun.*, **7**, 10266, <https://doi.org/10.1038/ncomms10266>.